J|A|C|S
ARTICLES

Evidence for Increased Exchange Interactions with 5d Compared to 4d Metal Ions. Experimental and Theoretical Insights into the Ferromagnetic Interactions of a Series of Trinuclear [$\{M(CN)_8\}^{3-}/Ni^{II}$] Compounds ($M = Mo^V$ or W^V)

Diana Visinescu,[†,§] Cédric Desplanches,[†] Inhar Imaz,[†] Vincent Bahers,[†]
Rabindranath Pradhan,[†] Frederick A. Villamena,[†] Philippe Guionneau,[†] and
Jean-Pascal Sutter*,[†,‡]

Contribution from the Institut de Chimie de la Matière Condensée de Bordeaux−CNRS, Université Bordeaux 1, 87, Avenue Dr. Schweitzer, F-33608 Pessac, France, Laboratoire de Chimie de Coordination du CNRS, Université Paul Sabatier, 205 route de Narbonne, F-31077 Toulouse, France, and Institute of Physical Chemistry "I. G. Murgulescu", Romanian Academy, Splaiul Indepentei 202, 060021 Bucharest, Romania

Received March 30, 2006; E-mail: sutter@lcc-toulouse.fr

Abstract: Two main questions are addressed in this study: (i) What increase of exchange interaction can be expected when replacing a paramagnetic metal ion with a heavier congener located farther down the periodic table (i.e., 3d−4d−5d), and (ii) for a molecular unit with higher coordination numbers, eight in the present case, how is the magnetic information transferred from the metal ion to its ligand set? Qualitative and quantitative investigations on a series of trimetallic cyano-bridged $\{Mo^V(CN)_8{-}Ni^{II}\}$ and $\{W^V(CN)_8{-}Ni^{II}\}$ compounds revealed ferromagnetic interactions but with a strength modulated by the spin organization and their nature. DFT calculations have been used to examine the mechanism and strengths of the exchange coupling, as well as the influence of the local symmetry of the cyanometalate unit on the spin density distribution. Both the experimental and the calculated behaviors underline a noticeable difference between the Mo and the W derivatives ($J_{MoNi} = 26.9$ cm^{-1} and $J_{WNi} = 37.3$ cm^{-1}) that is correlated to the spin density transferred from the metal center to its ligand set. It is also shown that the shape of the $\{M(CN)_8\}$ polyhedron may lead to nonequivalent CN sites and, consequently, to different strengths of the exchange interaction as a result of the position of the bridging ligands.

Introduction

Paramagnetic 4d and 5d transition metal ions have been recognized recently as very appealing spin carriers for the preparation of magnetic supramolecular architectures.[1] These ions are characterized by more radially extended valence orbitals compared with their 3d congeners, a trend following the sequence 5d > 4d ≫ 3d. To magneto-chemists, a more diffuse, singly occupied orbital suggests that an enhanced exchange interaction might be expected between interacting magnetic centers.[2] Spin−orbit coupling is also often observed for these ions, which makes them appealing building blocks for magnetic architectures. For instance, the use of paramagnetic 4d/5d cyanometalates, i.e., $\{Mo(CN)_7\}^{4-}$ and $\{M(CN)_8\}^{3-/4-}$ (with $M = Nb^{IV}$, Mo^V, or W^V), afforded, by association with 3d metal ions, extended 3-D networks exhibiting remarkable magnetic features and characterized by magnetic orders for temperatures as high as 106 K.[3−13] Numerous architectures of lower dimensionality have also been obtained with these modules, including high spin clusters.[14−20] Surprisingly, very little quantitative information concerning the strengths of the exchange interactions for cyano-bridged heterometallic compounds involving 4d or 5d metal ions is available.[16,21−25] The reason for this lack of data might be found in the complexity of the heteronuclear assemblies reported so far that impedes the numerical analysis of their magnetic behaviors. Knowledge about the sign and strength of the exchange parameter for a given spin system is, however, highly desirable not only for fundamental reasons but also to better understand, model, or design the magnetic behavior of more complex organizations. Furthermore, the 5d orbitals are more diffuse than the 4d orbitals. Accordingly, a stronger exchange interaction is anticipated with an ion of the third series with respect to its congener positioned just above it in the periodic

---

[†] Université Bordeaux 1.

[‡] Université Paul Sabatier.

[§] Romanian Academy.

(1) Mathonière, C.; Sutter, J.-P.; Yakhmi, J. V. In *Magnetism: molecules to materials*; Miller, J. S., Drillon, M., Eds.; Wiley-VCH: Weinheim, 2002; Vol. 4, pp 1−40.

(2) Ruiz, E.; Rodriguez-Fortea, A.; Alvarez, S.; Verdaguer, M. *Chem. Eur. J.* **2005**, *11*, 2135−2144.

(3) Larionova, J.; Clérac, R.; Sanchiz, J.; Kahn, O.; Golhen, S.; Ouahab, L. *J. Am. Chem. Soc.* **1998**, *120*, 13088−13095.

(4) Kahn, O.; Larionova, J.; Ouahab, L. *Chem. Commun.* **1999**, 945−952.

(5) Pilkington, M.; Decurtins, S. *Chimia* **2000**, *54*, 593−601.

(6) Zhong, Z. J.; Seino, H.; Mizobe, Y.; Hidai, M.; Verdaguer, M.; Ohkoshi, S.-I.; Hashimoto, K. *Inorg. Chem.* **2000**, *39*, 5095−5001.

(7) Larionova, J.; Clérac, R.; Donnadieu, B.; Guérin, C. *Chem. Eur. J.* **2002**, *8*, 2712−2716.

(8) Herrera, J. M.; Bleuzen, A.; Dromzée, Y.; Julve, M.; Lloret, F.; Verdaguer, M. *Inorg. Chem.* **2003**, *42*, 7052−7059.

(9) Tanase, S.; Tuna, F.; Guionneau, P.; Maris, T.; Rombaut, G.; Mathonière, C.; Andruh, M.; Kahn, O.; Sutter, J.-P. *Inorg. Chem.* **2003**, *42*, 1625−1631.

10.1021/ja061911x CCC: $33.50

Chart 1

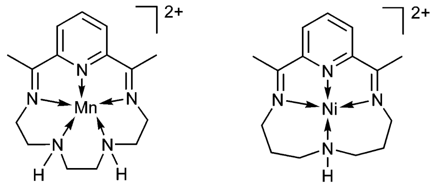

[MnL^1] [NiL^2]

table, but what will be the difference in terms of the exchange parameter remains to be established.

Herein, we report on qualitative and quantitative insights into the exchange interaction involving 4d or 5d metal ions in cyano-bridged complexes. Two series of novel trimetallic assemblies have been prepared and investigated, namely $[\{NiL^2(H_2O)\}_2\{M(CN)_8\}]^+$ (**1**) and $[\{NiL^2\}\{M(CN)_8\}_2]^{4-}$ (**2**), where M stands for Mo^V or W^V, and L^2 is a macrocyclic ligand (Chart 1). In all cases, the {Ni−Mo} and {Ni−W} exchange interactions have been found to be ferromagnetic but with a strength modulated by the spin organization and their nature. DFT calculations have been used to investigate the origin of the ferromagnetic interaction and its strength, as well as the influence of the symmetry of the cyanometalate unit on the spin density distribution. Both the experimental and the calculated behaviors underline a noticeable difference between the Mo and the W derivatives that can be correlated to the spin densities transferred by these metal ions onto the bridging cyano ligands. They also reveal that, when the polyhedron possesses nonequivalent CN sites, as is the case for a dodecahedron, the strength of the exchange interaction is significantly affected by the location of the bridging ligands.

Results and Discussion

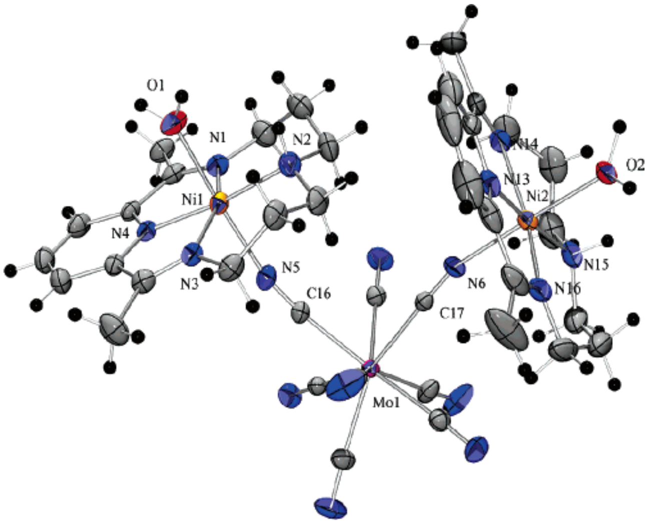

Figure 1. ORTEP view (30% probability level) of the cationic trinuclear $[\{NiL^2\}_2\{M(CN)_8\}]^+$ unit of compounds **1a** and **1b**. Selected interatomic distances (Å) and angles (°): for $[\{NiL^2(H_2O)\}_2\{Mo(CN)_8\}](ClO_4)$ (**1a**), Ni1−N1 2.069(3), Ni1−N2 2.008(3), Ni1−N3 2.029(3), Ni1−N4 1.951(3), Ni1−N5 2.129(4), Ni1−O1 2.163(3), Ni2−N13 1.948(4), Ni2−N14 2.031(4), Ni2−N15 2.023(4), Ni2−N16 2.052(4), Ni2−N6 2.101(3), Ni2−O2 2.163(3), Mo1−C16 2.167(4), Mo1−C17 2.166(4), Mo−C$_{CN}$(mean) 2.160, Ni1−Mo1 5.364(13), Ni2−Mo1 5.343(8), Ni1−N5−C16 164.4(3), Ni2−N6−C17 164.6(3), Mo1−C16−N5 173.3(4), Mo1−C17−N6 176.8(4), Ni1−Mo1−Ni2 85.50(1); for $[\{NiL^2(H_2O)\}_2\{W(CN)_8\}](ClO_4)$ (**1b**), Ni1−N1 2.035(10), Ni1−N2 2.067(10), Ni1−N3 2.033(12), Ni1−N4 1.949(10), Ni1−N5 2.134(13), Ni1−O1 2.193(10), Ni2−N13 1.950(11), Ni2−N14 2.035(11), Ni2−N15 2.030(14), Ni2−N16 2.058(12), Ni2−N6 2.116(12), Ni2−O2 2.211(8), W1−C16 2.180(16), W1−C17 2.178(10), W−C$_{CN}$(mean) 2.181, Ni1−W1 5.375(6), Ni2−W1 5.344(2), Ni1−N5−C16 165.0(9), Ni2−N6−C17 163.6(1), W1−C16−N5 173.9(1), W1−C17−N6 177.9(1), Ni1−W1−Ni2 85.85(2). (Further data can be found in the Supporting Information.)

Synthesis and Crystal Structures. The formation of low-dimensional assemblies with cyanometalates is usually achieved by employing cationic metal complexes bearing capping ligands that inhibit growth of extended coordination networks.[26,27] We have shown recently that $\{ML\}^{2+}$ units of paramagnetic 3d ions with all the equatorial coordination sites blocked by a macrocyclic ligand are well suited building blocks to form low-dimensional aggregates with octacyanometalates. Interestingly, the resulting architecture can be directed by the second partner of the reaction, i.e., $\{MnL^1\}^{2+}$ or $\{NiL^2\}^{2+}$ (Chart 1). For instance, when $\{Nb^{IV}(CN)_8\}^{4-}$ was associated with $\{NiL^2\}^{2+}$, an octadecanuclear aggregate was formed, while a 1-D polymeric structure has been obtained with $\{MnL^1\}$.[19] This prompted us to envisage the $\{NiL^2\}^{2+}$ unit to synthesize exchange-coupled heteronuclear compounds of small nuclearity with the paramagnetic cyanometalate modules $\{Mo^V(CN)_8\}^{3-}$ and $\{W^V(CN)_8\}^{3-}$.

The reaction of 2 equiv of $\{NiL^2\}^{2+}$ and 1 equiv of either $\{Mo^V(CN)_8\}^{3-}$ or $\{W^V(CN)_8\}^{3-}$ in the presence of perchloric acid (pH ∼2−3) afforded the trinuclear compound $[\{NiL^2(H_2O)\}_2\{M(CN)_8\}](ClO_4)$ (**1**: M = Mo^V, **1a**; W^V, **1b**). The same reaction carried out in the absence of $HClO_4$ or at pH > 3 was found to yield $[\{NiL^2\}\{M(CN)_8\}_2]\{NiL^2(H_2O)_2\}_2$ (**2**: M^V = Mo^V, **2a**; W^V, **2b**). These compounds could be obtained as either microcrystalline powders or larger single crystals, depending on the reaction procedure. Both **1a**,**b** and **2a**,**b** consist of charged trimetallic aggregates, where $\{M^V(CN)_8\}^{3-}$ and $\{NiL^2\}^{2+}$ units are linked by cyano groups but with a different stoichiometry and organization (Figures 1 and 2). The reactions have been performed in a slightly acidic medium to stabilize

---

(10) Arimoto, Y.; Ohkoshi, S.-I.; Zhong, Z. J.; Seino, H.; Mizobe, Y.; Hashimoto, K. *J. Am. Chem. Soc.* **2003**, *125*, 9240.
(11) Song, Y.; Ohkoshi, S.; Arimoto, Y.; Seino, H.; Mizobe, Y.; Hashimoto, K. *Inorg. Chem.* **2003**, *42*, 1848−1856.
(12) Le Goff, X. F.; Willemin, S.; Coulon, C.; Larionova, J.; Donnadieu, B.; Clérac, R. *Inorg. Chem.* **2004**, *43*, 4784−4786.
(13) Kashiwagi, T.; Ohkoshi, S.; Seino, H.; Mizobe, Y.; Hashimoto, K. *J. Am. Chem. Soc.* **2004**, *126*, 5024−5025.
(14) Larionova, J.; Gross, M.; Pilkington, M.; Andres, H.; Stoeckli-Evans, H.; Güdel, H. U.; Decurtins, S. *Angew. Chem., Int. Ed.* **2000**, *39*, 1605−1609.
(15) Zhong, Z. J.; Seino, H.; Mizobe, Y.; Hidai, M.; Fujishima, A.; Ohkoshi, S.-I.; Hashimoto, K. *J. Am. Chem. Soc.* **2000**, *122*, 2952−2953.
(16) Podgajny, R.; Desplanches, C.; Sieklucka, B.; Sessoli, R.; Villar, V.; Paulsen, C.; Wernsdorfer, W.; Dromzée, Y.; Verdaguer, M. *Inorg. Chem.* **2002**, *41*, 1323−1327.
(17) Bonadio, F.; Gross, M.; Stoeckli-Evans, H.; Decurtins, S. *Inorg. Chem.* **2002**, *41*, 5891−5896.
(18) Sieklucka, B.; Podgajny, R.; Korzeniak, T.; Przychodzen, P.; Kania, R. *C. R. Chim.* **2002**, *5*, 639−649.
(19) Pradhan, R.; Desplanches, C.; Guionneau, P.; Sutter, J.-P. *Inorg. Chem.* **2003**, *42*, 6607−6609.
(20) Song, Y.; Zhang, P.; Ren, X.-M.; Shen, X.-F.; Li, Y.-Z.; You, X.-Z. *J. Am. Chem. Soc.* **2005**, *127*, 3708−3709.
(21) Li, D.; Gao, S.; Zheng, L.; Yu, K.; Tang, W. *New J. Chem.* **2002**, *26*, 1190−1195.
(22) Sokol, J. J.; Hee, A. G.; Long, J. R. *J. Am. Chem. Soc.* **2002**, *124*, 7656−7657.
(23) Shores, M. P.; Sokol, J. J.; Long, J. R. *J. Am. Chem. Soc.* **2002**, *124*, 2279−2292.
(24) Beauvais, L. G.; Long, J. R. *J. Am. Chem. Soc.* **2002**, *124*, 2110−2111.
(25) Przychodzen, P.; Lewinski, K.; Balanda, M.; Pelka, R.; Rams, M.; Wasiutynski, T.; Guyard-Duhayon, C.; Sieklucka, B. *Inorg. Chem.* **2004**, *43*, 2967−2974.
(26) Marvaud, V.; Decroix, C.; Sculler, A.; Tuyèras, F.; Guyard-Duhayon, C.; Vaissermann, J.; Marrot, J.; Gonnet, F.; Verdaguer, M. *Chem. Eur. J.* **2003**, *9*, 1692−1705.
(27) Lescouëzec, R.; Toma, L. M.; Vaissermann, J.; Verdaguer, M.; Delgado, F. S.; Ruiz-Pérez, C.; Lloret, F.; Julve, M. *Coord. Chem. Rev.* **2005**, *249*, 2691−2729.

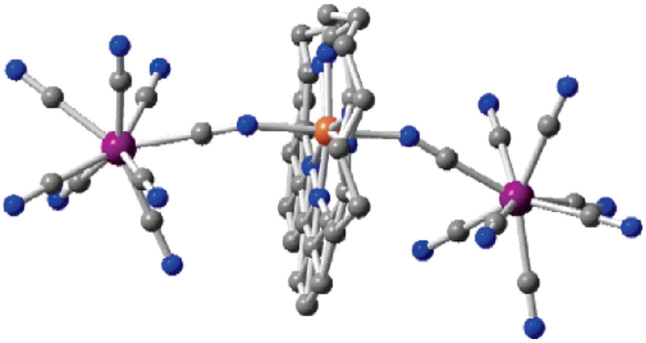

Figure 2. View of the anionic $[\{NiL^2\}\{M(CN)_8\}_2]^{4-}$ aggregate of compounds **2** (M = Mo^V, **2a**; W^V, **2b**). (The macrocylic ligand of the central $\{NiL^2\}$ is highly disordered and could not be fixed.)

the cyanometalate units and to slow the assembly process in order to favor the crystals' growth. It is interesting to note that a $HClO_4$ concentration above 10^{-3} mol·L^{-1} had a dramatic effect on the course of the reaction and directed the assembly process to a different product. This may be attributed to the associated anion rather than to the proton. The relative concentration of ClO_4^- may indeed influence the solubility of some of the species in equilibrium in the solution and therefore drive the crystallization of one product out of the reaction mixture.[11,26]

The crystal structures for compounds **1a** and **1b** have been solved and found to be isostructural (Table 1). They consist of a cationic heterotrinuclear $[\{NiL^2(H_2O)\}_2\{M(CN)_8\}]^+$ unit counterbalanced by a ClO_4^- anion. A view of the trinuclear aggregate is depicted in Figure 1; the ORTEP plot and complete numbering scheme for **1a** and **1b**, along with a listing of bond lengths and angles, can be found as Supporting Information. This trinuclear moiety consists of one octacyanometalate module linked to two $\{NiL^2\}$ units organized in a cis arrangement. The Ni atoms are hexacoordinated, with a distorted octahedral stereochemistry. The equatorial planes of the polyhedra are determined by the four atoms of the macrocyclic ligand, while the apical positions are occupied by an N-bound cyano group and a water molecule, respectively. The Mo/W−CN→Ni linkages are slightly bent, with mean angles of 175.05° (**1a**) and 175.72° (**1b**) for M−C−N, and 164.50° (**1a**) and 164.27° (**1b**) for the Ni−N−C moieties. The crystal packing diagram for **1a**,**b** reveals a hydrogen-bonding network involving the coordinated H_2O of the trinuclear moiety and one N atom belonging to the CN groups, as well as the solvate H_2O molecules. Each trinuclear unit is linked to a neighboring unit by a H-bond established between O−H2B and N10 (O2···N10 = 2.872(8) Å for **1a** and 2.853(9) Å for **1b**), setting up a 1-D organization (see Supporting Information).

Table 1. Experimental and Crystal Data

	1a	1b
empirical formula	$C_{38}H_{48}N_{16}Ni_2O_2Mo\cdot ClO_4\cdot 4H_2O$	$C_{38}H_{48}N_{16}Ni_2O_2W\cdot ClO_4\cdot 3H_2O$
crystal system	monoclinic	
space group	$P2_1/n$	
Z	4	
temperature (K)	293(2)	293(2)
formula weight (g·mol^{-1})	1137.7	1215.4
unit cell dimensions		
a (Å)	10.656(5)	10.667(1)
b (Å)	12.320(5)	12.301(1)
c (Å)	39.125(3)	39.293(4)
β (deg)	95.48(5)	95.53(3)
volume (Å^3)	5113(3)	5132(9)
D_X	1.478	1.573
F(000)	2332	2452
radiation	Mo Kα (λ = 0.71073 Å)	
monochromator	graphite	
diffractometer	Enraf-Nonius Kappa CCD	
absorption coefficient (mm^{-1})	1.089	3.078
crystal dimension (mm^3)	0.25 × 0.25 × 0.02	0.4 × 0.35 × 0.02
θ range (°)	3.5−26.4	1−25.1
index ranges	$-13 \leq h \leq 13$ $-15 \leq k \leq 15$ $-47 \leq l \leq 48$	$-8 \leq h \leq 8$ $-15 \leq k \leq 15$ $-45 \leq l \leq 45$
scan type	CCD scans	
reflections collected [$I > 2\sigma(I)$]	10397	16670
independent reflections [$I > 2\sigma(I)$]	6241	8580
refinement method	full-matrix least-squares on F^2	
parameters refined	649	604
weighting scheme	$w = 1/[\sigma^2(F_o^2) + (\alpha P)^2 + \beta P]$, where $P = (F_o^2 + 2F_c^2)/3$	
absorption correction	SCALEPACK	
goodness-of-fit on F^2	1.02	1.21
final R indices [$I > 2\sigma(I)$]		
R_1	0.049	0.056
wR_2	0.117	0.177
maximum shift/esd	<0.001	<0.001

For both **2a** and **2b**, the macrocyclic ligand of the central Ni unit was found to be strongly disordered, which results in a rather poor quality of the structure solutions as far as this fragment is concerned (for crystal data, see Experimental Section). Nevertheless, the general structural organization is well fixed and consists of the anionic heterotrinuclear aggregate $[\{NiL^2\}\{M(CN)_8\}_2]^{4-}$ (Figure 2) associated with two independent $\{NiL^2(H_2O)_2\}^{2+}$ cations acting as counterions. Two $\{M(CN)_8\}^{3-}$ units are linked through one of their cyano ligands to the apical positions of a $\{NiL^2\}^{2+}$ module to form a linear trinuclear moiety. Although all the M^V−C−N angles are close to 180° (177.5−178.8° for **2b**), the C−N→Ni angles significantly deviate from linearity, with a value of 154.4° for **2b**. The crystal packing reveals a hydrogen bond network among the anionic aggregates and the cationic moieties. These bonds are established between the coordinated H_2O and N atoms of terminal cyano ligands, setting up a 3-D network (see Supporting Information).

Magnetic Properties. The temperature dependences of the molar magnetic susceptibilities, χ_M, for **1a**,**b** and **2a**,**b** have been investigated in the temperature domain 2−300 K. The variations of $\chi_M T$ versus T for the two isomorphous complexes $[\{NiL^2(H_2O)\}_2\{M(CN)_8\}](ClO_4)$ (**1a**, M = Mo^V, and **1b**, M = W^V) are depicted in Figure 3. The value of $\chi_M T$ at 300 K for each compound, i.e., 2.78 cm^3·K·mol^{-1} for **1a** and 2.75 cm^3·K·mol^{-1} for **1b**, is in good agreement with the anticipated value of 2.58 cm^3·K·mol^{-1} for two Ni^{II} ions ($S = 1$, $g = 2.1$) and one Mo^V or W^V ion ($S = {}^1/_2$, $g = 2$) without interactions. These values increase as temperature diminishes, reaching maximum values of 3.48 cm^3·K·mol^{-1} (**1a**) and 3.67 cm^3·K·mol^{-1} (**1b**) at 19−20 K before decreasing rapidly at lower temperatures. The profile of the curves clearly reveals that ferromagnetic $\{Ni^{II}-Mo^V\}$ and $\{Ni^{II}-W^V\}$ interactions take place, in agreement with earlier observations.[17,28] The steep decrease of $\chi_M T$ in the low-temperature domain is attributed to intermolecular interactions likely to be mediated by the hydrogen bonds linking these aggregates in the crystal rather than to zero-field splitting because the $\chi_M T$ values reached for the rounded maximum are

---

[28] Ferromagnetic interaction was also observed for Mo(III); see ref 23.

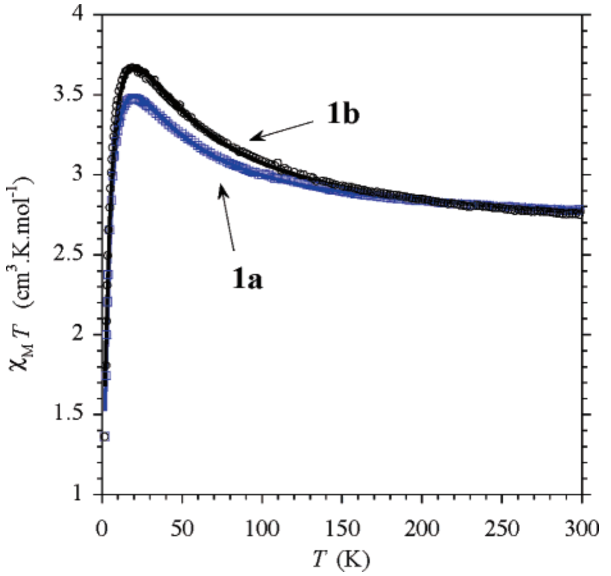

Figure 3. Experimental (□/○) and calculated (—) temperature dependence of $\chi_M T$ for complexes $[\{NiL^2(H_2O)\}_2\{M(CN)_8\}](ClO_4)$ (**1a**, □, M = Mo^V; **1b**, ○, M = W^V). Best-fit parameters: for **1a**, $J_{MoNi} = 26.9 \pm 0.2$ cm^{-1}, $zJ' = -1.0$ cm^{-1}, $g_{Ni} = 2.14$, and $g_{Mo} = 2$ (fixed); for **1b**, $J_{WNi} = 37.3 \pm 0.6$ cm^{-1}, $zJ' = -0.86$ cm^{-1}, $g_{Ni} = 2.11$, and $g_W = 2$ (fixed).

much below the 4.375 cm^3·K·mol^{-1} expected for an $S = {}^5/_2$ ground state. Moreover, attempts to fit this curve by replacing the zJ' term by an anisotropy factor $D_{5/2}$ on the ground state $S = {}^5/_2$ leads to bad quality adjustments and unrealistic D values.

The interaction parameter between Mo^V and Ni^{II} was determined from least-squares fitting of the theoretical expression given in eq 1, deduced from the spin Hamiltonian $\boldsymbol{H} = -J(\mathbf{S}_{Ni1}\cdot\mathbf{S}_{Mo} + \mathbf{S}_{Ni2}\cdot\mathbf{S}_{Mo}) + \beta[g_{Ni}(\mathbf{S}_{Ni1} + \mathbf{S}_{Ni2}) + g_{Mo}\mathbf{S}_{Mo}]\mathbf{H}$.

$$\chi_M T = \frac{\chi_{M(mol)}T}{1 - \dfrac{zJ'\chi_{M(mol)}}{Ng^2_{S',S}\beta^2}} \qquad (1)$$

with

$$\chi_{M(mol)}T = \frac{N\beta^2}{3k} \times \left[\left\{\frac{52.5(28g_{Ni} + 7g_M)^2}{(35)^2} + \frac{15(18g_{Ni} - 3g_M)^2}{(15)^2}\exp\left(-\frac{5J}{2kT}\right) + \frac{15(10g_{Ni} + 5g_M)^2}{(15)^2}\exp\left(-\frac{J}{2kT}\right) + \frac{1.5\,(4g_{Ni} - g_M)^2}{(3)^2}\exp\left(-\frac{2J}{kT}\right) + 1.5g_{M^2}\exp\left(-\frac{J}{kT}\right)\right\}\Bigg/ \left\{6 + 4\exp\left(-\frac{5J}{2kT}\right) + 4\exp\left(-\frac{J}{2kT}\right) + 2\exp\left(-\frac{2J}{kT}\right) + 2\exp\left(-\frac{J}{kT}\right)\right\}\right]$$

and

$$g_{S',S} = g_{1,5/2} = \frac{28g_{Ni} + 7g_M}{35}$$

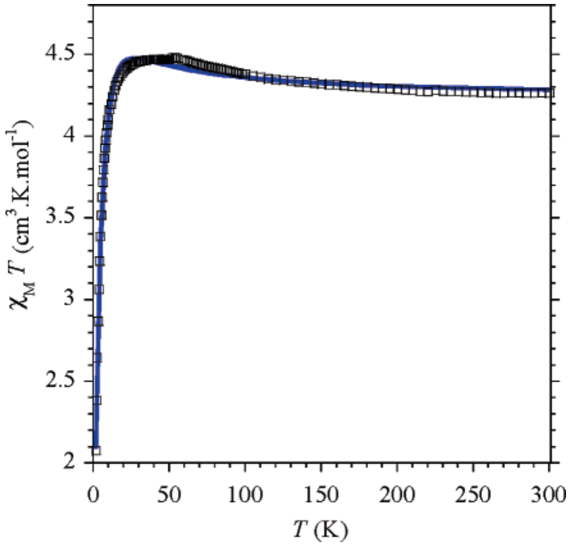

Figure 4. Experimental (□) and calculated (—) temperature dependence of $\chi_M T$ for complexes $[\{NiL^2\}\{Mo(CN)_8\}_2]\{NiL^2(H_2O)_2\}_2$ (**2a**). Best-fit parameters: for **2a**, $J_{MoNi} = 15.4 \pm 0.3$ cm^{-1}, $zJ' = -0.62$ cm^{-1}, $g_{Ni} = 2.116$, and $g_{Mo} = 2$ (fixed); for **2b**, $J_{WNi} = 14.2 \pm 0.3$ cm^{-1}, $zJ' = -0.74$ cm^{-1}, $g_{Ni} = 2.15$, and $g_W = 2$ (fixed).

To take into account the decrease of $\chi_M T$ below 20 K, weak intermolecular interactions based on the mean-field approximation, zJ', have been considered. The best fit to the experimental data of **1a** was obtained for $J_{MoNi} = 26.9 \pm 0.2$ cm^{-1}, $zJ' = -1.0$ cm^{-1}, $g_{Ni} = 2.14$, and $g_{Mo} = 2$ (fixed). The same analysis applied to the behavior of the W derivative **1b** yielded $J_{WNi} = 37.3 \pm 0.6$ cm^{-1}, $zJ' = -0.86$ cm^{-1}, $g_{Ni} = 2.11$, and $g_W = 2$ (fixed) (Figure 3).

The overall magnetic behaviors of $[\{NiL^2\}\{M(CN)_8\}_2]\{NiL^2(H_2O)_2\}_2$ (**2a**, M^V = Mo^V, and **2b**, M^V = W^V) are similar to those observed for **1a**,**b** (Figure 4 and Supporting Information). The values found for $\chi_M T$ at 300 K are 4.26 and 4.21 cm^3·K·mol^{-1} for **2a** and **2b**, respectively, in good agreement with the expected value of 4.05 cm^3·K·mol^{-1} for three Ni^{II} and two Mo^V/W^V noncorrelated ions. These values increase slightly at lower temperatures, describing a broad maximum with 4.47 and 4.35 cm^3·K·mol^{-1}, and $\chi_M T$ abruptly decreases below 30 K. Here again, intramolecular ferromagnetic Ni^{II}−Mo^V and Ni^{II}−W^V interactions are operative with weaker intermolecular antiferromagnetic interactions.

Numerical analysis of these behaviors was done with the theoretical expression of the magnetic susceptibility, $\chi_{M(mol)}$, for the pentanuclear system given in eq 2.

$$\chi_{M(mol)}T = \frac{N\beta^2}{3k} \times \left[\frac{30g^2_{1/2} + 6g^2_{Ni}\exp\left(-\frac{J}{kT}\right) + 6g^2_{1/2}\exp\left(-\frac{2J}{kT}\right)}{5 + 3\exp\left(-\frac{J}{kT}\right) + 3\exp\left(-\frac{2J}{kT}\right) + \exp\left(-\frac{3J}{kT}\right)}\right] + 4g^2_{Ni} \qquad (2)$$

with

$$g_{1/2} = \frac{g_M + g_{Ni}}{2}$$

This expression takes into account the Ni−Mo/W exchange interactions deduced from the spin Hamiltonian $\boldsymbol{H} = -J\mathbf{S}_{Ni}\cdot(\mathbf{S}_{M1} + \mathbf{S}_{M2}) + \beta[g_M(\mathbf{S}_{M1} + \mathbf{S}_{M2}) + g_{Ni}\mathbf{S}_{Ni}]\mathbf{H}$ and the paramagnetic contribution of two Ni^{II} ions. The intermolecular interactions have been considered within the mean-field approximation (eq 1 with $g_{S',S} = 2$). Least-squares fitting to the experimental data yielded for **2a** $J_{MoNi} = 15.4 \pm 0.3$ cm^{-1}, $zJ' = -0.62$ cm^{-1}, $g_{Ni} = 2.16$, and $g_{Mo} = 2$ (fixed), and for **2b** $J_{WNi} = 14.2 \pm 0.3$ cm^{-1}, $zJ' = -0.74$ cm^{-1}, $g_{Ni} = 2.15$, and $g_W = 2$ (fixed).The magnetic behaviors of these four compounds show that the {Ni−Mo^V} and {Ni−W^V} interactions are ferromagnetic but also reveal important differences in the magnitude of the exchange couplings. Most important is the significant increase of the exchange interaction for the W compound **1b** as compared to the Mo derivative **1a**, with respectively $J_{WNi} = 37.3 \pm 0.6$ cm^{-1} and $J_{MoNi} = 26.9 \pm 0.2$ cm^{-1}. This difference between the Mo and W is not seen for **2a**,**b**, and the exchange parameters for these compounds are much smaller than for **1a**,**b**. At first glance, the weaker interactions could be ascribed to the Ni←NC angle (164.3°) that deviates significantly from linearity. Moreover, a theoretical investigation suggests that, for a given set of molecular units, the exchange interaction is influenced by the spin topology.[29] Finally, the geometry of the {$M(CN)_8$} and the site of the CN linking the metal center might be crucial as well (vide infra).

In the forthcoming sections, we present the results of the DFT study undertaken to gain some insight into the origin of the magnetic behaviors exhibited by these compounds. To evaluate the impact of the geometry of the {$M(CN)_8$} unit on the magnetic behavior, we have compared the case of **1a**,**b** to reference geometries of an eight-vertex polyhedron. The transfer of the magnetic information from the metal ion to the CN ligands has been examined in term of spin population by means of DFT calculations performed for both reference geometries and the actual shape of {$M(CN)_8$} in **1**.

The geometry of the paramagnetic {$M(CN)_8$} unit (Mo^V, W^V, Nb^{IV}, ...) is rarely considered when the magnetic behaviors of heteronuclear compounds involving these building units are discussed. It is usually believed that the magnetic information is transferred equally from the central metal ion to each of the eight cyanide ligands, in much the same way as for {$Cr(CN)_6$}$^{3-}$. This is not necessarily true. The metal ions of these units have a d^1 electronic configuration with an $S = {}^1/_2$ spin ground state. As a result, there is usually a single magnetic orbital, the type of which is directly dependent on the geometry of the {$M(CN)_8$}$^{3-}$ unit.[30] The overlap between the ligand orbitals and the magnetic orbital of the ion, the rationale for the strength of the magnetic interaction, and its nature may therefore be dependent on the actual shape of {$M(CN)_8$}.

Geometry of the Octacyanometalates. It is recognized that octacyanometalates have three stable limit geometries, namely the square antiprism (SAP, D_{4d}), the dodecahedron (DD, D_{2d}), and the bicapped trigonal prism (BTP, C_{2v}). The first two geometries are depicted in Figure 5. Deviations from these ideal geometries are generally discussed in terms of dihedral angles δ and ϕ.[31] To define these angles, a polyhedral structure formed by the atoms of the first coordination sphere of the metal is defined. The connections of these atoms thus delineate the faces of the polyhedron. All these faces are equilateral triangles or nearly so. The δ angles are defined as dihedral angles between the normals of adjacent triangles. The SAP, DD, and BTP polyhedra all have 8 vertexes, 12 faces, and 18 edges. Thus, for any model or experimental polyhedron, 18 values of δ can be calculated. However, it is normally sufficient to define a subset of 4 δ values to characterize the deviation of an experimental geometry from the model geometry. For DD and SAP geometries, the edges used to define the subset of δ values are shown with gray lines in Figure 5. A dodecahedron is also characterized by the intersection of two orthogonal trapezoids (AABB in Figure 5). Distortions from the ideal dodecahedral shape lead to a twisting of these planes. The nonplanarity of the trapezoidal-type atoms, defined by the angle ϕ,[32] is another useful parameter for characterizing eight-atom polyhedra. The values of δ and ϕ for the model geometries and the geometry occurring in **1** and **2** are gathered in Table 2. Comparison of these values indicates that the shape of the {$M(CN)_8$} unit in **1** and **2** corresponds to none of the reference geometries defined above. All the 18 δ angles found for **1** have values equal to or higher than 18.8°. Obviously, this rules out a shape close to the SAP and BTP, for which at least one δ angle is equal to zero. Closest is the DD geometry, with a maximum deviation of 11.7° for the δ angle. This is also supported by the ϕ angles. The same analysis applies for **2**, with a deviation of less than 9.3° for the δ angles. The polyhedron defining the {$M(CN)_8$} unit in **1** and **2** is thus best described by a slightly distorted dodecahedron geometry. To confirm this conclusion and to obtain quantitative parameters to evaluate the deviation of these polyhedra from the ideal symmetry, a *continuous shape measures* (CShM) analysis was performed.[33−36] The evaluation

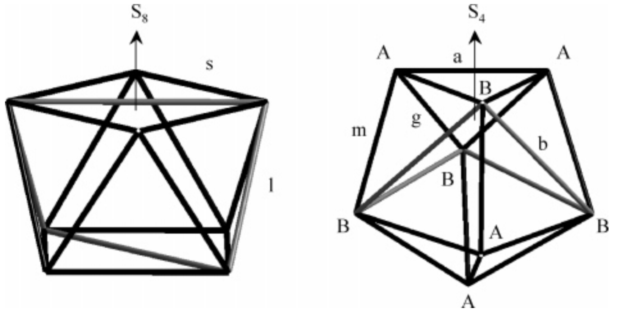

Figure 5. Square antiprism (left) and dodecahedron (right) geometries. (In hard-sphere model, $s = l$ for a square antiprism and $g = m = a$, $b = 1.250a$ for a dodecahedron.)

Table 2. δ and ϕ Angles (Deg) for Model and Experimental Eight-Vertex Geometries

geometry	δ	ϕ
SAP	0.0, 0.0, 52.4, 52.4	24.5
BTP	0.0, 21.8, 48.2, 48.2	14.1
DD	29.5, 29.5, 29.5, 29.5	0.0
{$M(CN)_8$} in **1**	35.5, 18.8, 40.7, 28.6	5.2, 7.8
{$M(CN)_8$} in **2**	20.2, 38.0, 33.7, 30.2	4.7, 5.6

---

(29) Raghunathan, R.; Sutter, J.-P.; Ducasse, L.; Desplanches, C.; Ramasesha, S. *Phys. Rev. B* **2006**, *73*, 104438.
(30) Perumareddi, J. R.; Liehr, A. D.; Adamson, A. W. *J. Am. Chem. Soc.* **1963**, *85*, 249−259.
(31) Muetterties, E. L.; Guggenberger, L. J. *J. Am. Chem. Soc.* **1974**, *96*, 1748−1756.
(32) ϕ is the dihedral angle between two triangles constructed from the trapezoid atoms, i.e., the triangles delineated by A−A and the middle of BB, and B−B and the middle of the AA edge (see ref 31).
(33) Alvarez, S.; Alemany, P.; Casanova, D.; Cirera, J.; Llunell, M.; Avnir, D. *Coord. Chem. Rev.* **2005**, *249*, 1693−1708.
(34) Casanova, D.; Llunell, M.; Alemany, P.; Alvarez, S. *Chem. Eur. J.* **2005**, *11*, 1479−1494.
(35) Casanova, D.; Cirera, J.; Llunell, M.; Alemany, P.; Avnir, D.; Alvarez, S. *J. Am. Chem. Soc.* **2004**, *126*, 1755−1763.
(36) Cirera, J.; Ruiz, E.; Alvarez, S. *Chem. Eur. J.* **2006**, *12*, 3162−3167.

Table 3. Results of the Continuous Shape Measure Analysis[a]

geometry	S_{DD}	S_{SAP}	S_{BTP}	$\Delta_{(DD,SAP)}$	$\varphi_{(DD>SAP)}$
$\{M(CN)_8\}$ in **1**	0.56	1.74	2.00	0.22	44%
$\{M(CN)_8\}$ in **2**	0.39	2.03	2.37	0.21	37%

[a] S_{DD} is the shape measure relative to the dodecahedron, S_{SAP} the shape measure relative to the square antiprism, and S_{BTP} the shape measure relative to the bicapped trigonal prism; $\Delta_{(DD,SAPR)}$ represents the deviation from the DD−SAPR interconversion path and $\varphi_{(DD>SAPR)}$ the generalized interconversion coordinate.[36]

of the deviation of the actual shape of the $\{M(CN)_8\}$ units in **1** and **2** from reference polyhedra is summarized in Table 3 in terms of the CShM parameter S, determined with respect to DD, SAP, and BTP polyhedra. The value taken by S is zero when the analyzed polyhedron exhibits exactly the reference geometry and increases with the degree of distortion. The values obtained for the $\{M(CN)_8\}$ units in **1** and **2** clearly show that they exhibit a geometry close to a dodecahedron, with $S_{DD} = 0.56$ for **1** and 0.39 for **2**, confirming the geometrical analysis. As a matter of comparison, the CShM analysis of a square antiprism with respect to the dodecahedron taken as reference yields $S_{DD} = 2.847$.[34] Moreover, the actual shape of the $\{M(CN)_8\}$ units is found to be close to the interconversion path between DD and SAP, as revealed by the small Δ values (Table 3). Thus, both the geometrical parameter analysis and the CShM show that, for **1** and **2**, the shape exhibited by the $\{M(CN)_8\}$ unit is a distorted DD geometry, the distortion being slightly smaller for **2** than for **1**. Because $\{M(CN)_8\}$ is most distorted for **1**, we have considered this actual geometry for the theoretical investigations described hereafter. Finally, it can be emphasized that, for **1**, the bridging cyanide ligands are located on B-type sites of the $\{M(CN)_8\}$ polyhedron (Figure 5), whereas they are found on A sites for **2**; this parameter is important, as will be seen below.

Shape of Molecular Orbital, Spin Density, and Spin Populations for $[M(CN)_8]^{3-}$: Comparison between Model and Experimental Geometries. The spacing of d orbitals in a crystal field is well established for SAP and DD geometry.[37] For our purpose, it is sufficient to remember that, for a d^1 electronic configuration, each geometry possesses a single, nondegenerate d orbital with lowest energy. This orbital is the d_{z^2} for the square antiprism geometry and the d_{xy} in a dodecahedron surrounding.[38] Going one step further, Hoffmann and co-workers[39] have scrutinized several eight-coordination geometries using the extended Hückel framework. For a dodecahedral geometry, the d_{xy} is σ nonbonding because all the ligand atoms are located in the nodal planes of this orbital (see Figure 6b). For a square antiprismatic geometry, the d_{z^2} orbital is σ nonbonding for $\theta = 54.73°$ (θ is the angle between the M−CN direction and the z axis); for larger and smaller values, it is slightly antibonding. The actual value in the ideal SAP structure of $\{M(CN)_8\}$ is $\theta = 59.26°$, but we do not expect the σ system to make a significant contribution in the description of the lowest d level in the antiprismatic structure. For both the DD and SAP geometries, the lowest d level essentially mixes with the π system of the cyanide ligands. Hoffmann and co-workers have also shown that, for the dodecahedral geometry, the overlap integral between the d_{xy} orbital of the metal ions and a so-called $\pi_\perp$ orbital of the ligand ($\perp$ indicates that the orbital is orthogonal to the nodal plane $x = 0$ or $y = 0$ in which the ligand is located) is given by the function $S(\theta) = S_\pi \sin\theta$. Thus, a better overlap is anticipated for the ligands located on the vertexes labeled B in Figure 5 ($\theta = 69.46°$) than for those positioned on the vertexes A ($\theta = 36.85°$). The d_{xy} being a singly occupied molecular orbital, a direct consequence of the better overlap should be a larger spin density on the atoms of the ligands in B. For the square antiprismatic structure, some overlap is expected between the d_{z^2} orbital and the π system of the cyanides, the overlap being maximum for $\theta = 45°$. In this geometry, all the cyanides are equivalent.

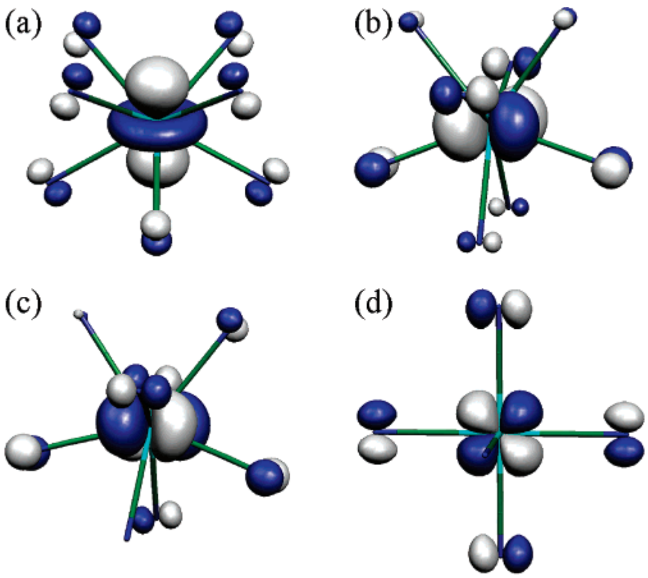

Figure 6. HOMOs for the $[Mo(CN)_8]^{3-}$ moiety in (a) square antiprismatic, (b) dodecahedral, and (c) experimental geometries. (d) One of the three HOMOs for the octahedral $[Cr(CN)_6]^{3-}$.

The DFT calculations performed on the $[Mo(CN)_8]^{3-}$ unit in SAP, DD, and experimental geometries (see Experimental Section) support all these statements. In Figure 6 are depicted the highest occupied molecular orbitals (HOMOs) obtained for $[Mo(CN)_8]^{3-}$ as well as for the $[Cr(CN)_6]^{3-}$ unit. It can be verified that, for all geometries, the involved d orbital of the metal ion is indeed the orbital that was anticipated. It is important to note that the HOMOs obtained for the geometry occurring in **1** and the DD geometry have very much the same shape. Clearly, the slight distortion from the DD geometry of the polyhedron of the $\{M(CN)_8\}$ unit in **1** does not modify the HOMO with respect to the HOMO of an ideal dodecahedral symmetry, as the unpaired electron of $\{M(CN)_8\}$ in **1** and **2** is located in the d_{xy} orbital of the central metal ion. The cyanides contribute to the HOMO through their π system and especially by a p orbital localized on the N atoms. The shape of the orbital on the cyanide is the same whether the overlap with the metal ion concerns the d_{z^2} or the d_{xy} orbitals for $[Mo(CN)_8]^{3-}$ or the t_{2g} orbital for $[Cr(CN)_6]^{3-}$. The contribution to the HOMO of the p orbitals can be attributed to a delicate balance between metal-to-ligand back-donation involving the empty CN π^*

---

(37) Ballhausen, C. J. *Introduction to ligand field theory*; McGraw-Hill Books Inc.: New York, 1962.

(38) For the dodecahedron, the label of the lowest energy d orbital depends on the orientation of the ligands. Some authors are placing the ligands on the planes $x + y = 0$ and $x - y = 0$, in such an orientation the lowest orbital is the $d_{x^2-y^2}$.

(39) Burdett, J. K.; Hoffmann, R.; Fay, R. C. *Inorg. Chem.* **1978**, *17*, 2553−2568.

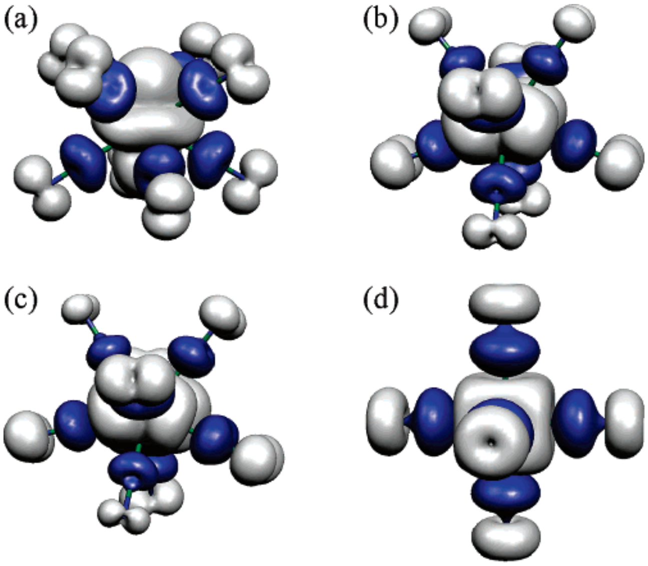

Figure 7. Distribution of spin density (positive in gray and negative in blue) deduced from DFT calculations for the $[Mo(CN)_8]^{3-}$ moiety in various geometries: (a) square antiprismatic, (b) dodecahedral, and (c) actual shape in compound **1**. (d) Spin density distribution computed for the octahedral $[Cr(CN)_6]^{3-}$.

orbitals and a repulsive interaction with the occupied π orbitals of the CN units.[40]

The spin density distributions computed for each case are depicted in Figure 7. The areas of positive density (in gray) have the same shapes as the HOMOs. In addition, some negative spin density is observed on the C atoms as a result of spin polarization. The spin populations have been analyzed using the NBO method.[41] For the determination of the σ and π parts of the spin density for cyanides, these have been oriented along a local z axis. With this orientation, the σ system is composed of 2s and $2p_z$ orbitals, whereas $2p_x$ and $2p_y$ orbitals constitute the π system.

The spin populations for $[Mo(CN)_8]^{3-}$ in SAP and DD geometries as well as for the geometry occurring in **1** for Mo and W are summarized in Table 4. The small difference between the sum of σ and π spin densities and the total spin density is due to small amounts of spin in core and polarization orbitals. The results obtained for the octahedral $[Cr(CN)_6]^{3-}$ are also given. It is gratifying that the spin density distribution for $[Cr(CN)_6]^{3-}$ deduced from these calculations is in reasonable agreement with that deduced from polarized neutron diffraction experiments (see Table 4).[42] In all cases, the spin density on the nitrogen atom of the CN ligands is mainly localized in the π orbitals, whereas the spin density on the C atoms is issued from both σ and π orbitals. The anticipated difference between the ligand sites A and B for the DD and experimental geometries is observed: a notably larger spin density is found on the CN located on vertexes B. It can be noticed also that no significant difference is found between the experimental and DD geometries for the values of σ and π spin on the cyanides. This suggests that the distortion of the polyhedron is not sufficient to alter the orbital overlap. For the SAP geometry, the spin density located on the N atoms is significantly lower (35%) than the spin found for N_B in DD but larger than that for the N_A sites. Most interesting is the comparison of the results obtained for $[Mo(CN)_8]^{3-}$ and $[W(CN)_8]^{3-}$. The spin density found on the ligands for the W derivative is significantly larger than that for the Mo unit. Finally, it can be mentioned that, for both the $[Mo(CN)_8]^{3-}$ (in **1a** or DD geometry) and $[Cr(CN)_6]^{3-}$ units, the spin densities found at the N atoms are in the same range, despite the fact that Cr^{III} has a spin state of $S = {}^3/_2$, whereas Mo^V has only spin $S = {}^1/_2$.

Table 4. Spin Density Distributions Obtained for $[Mo(CN)_8]^{3-}$, $[W(CN)_8]^{3-}$, and the Octahedral $[Cr(CN)_6]^{3-}$ Unit

	atom[a]	total spin density[b]	σ spin density	π spin density
SAP $\{Mo(CN)_8\}^{3-}$	Mo	+0.9103		
	C	−0.0313	−0.0143	−0.0186
	N	+0.0425	+0.0004	+0.0423
DD $\{Mo(CN)_8\}^{3-}$	Mo	+0.9021		
	C_A	−0.0264	−0.0145	−0.0124
	C_B	−0.0407	−0.0165	−0.0274
	N_A	+0.0267	−0.0002	+0.0270
	N_B	+0.0649	+0.0010	+0.0640
$\{Mo(CN)_8\}^{3-}$ in **1**	Mo	+0.898		
	C_A	−0.0264	−0.0144	−0.0126
	C_B	−0.0394	−0.0151	−0.0271
	N_A	+0.0269	−0.0002	+0.0272
	N_B	+0.0644	+0.0010	+0.0636
$\{W(CN)_8\}^{3-}$ in **1**	W	+0.825		
	C_A	−0.0244	−0.0113	−0.0141
	C_B	−0.0416	−0.0138	−0.0317
	N_A	+0.0322	+0.0003	+0.0319
	N_B	+0.0776	+0.0015	+0.0761
octahedral $[Cr(CN)_6]^{3-}$	Cr	+3.0426		
		(+3.25)[c]		
	C	−0.0757	−0.0375	−0.0393
		(−0.088)[c]	(−0.044)[c]	(−0.044)[c]
	N	+0.0686	+0.0001	+0.0686
		(+0.053)[c]	(−0.034)[c]	(+0.087)[c]

[a] The labels A and B refer to the positions given in Figure 5. [b] For the DD and the experimental geometries, the spin density given for C and N atoms is the mean value of the four atoms located at either site A or B. [c] The values given in parentheses are the spin densities obtained from neutron diffraction studies.[42]

Computed Exchange Coupling and Pathway. For **1**, the two bridging cyanides are located on B-type sites, and the structural features of the $\{Mo-CN\rightarrow NiL^2\}$ fragments are nearly identical. Therefore, the exchange interaction parameter J has been calculated for a dinuclear fragment $[Ni(L^2)(H_2O)][Mo(CN)_8]^-$ (with the Ni1 moiety from the structural data) of the trinuclear $[\{NiL^2(H_2O)\}_2\{Mo(CN)_8\}]^+$ (**1**). Calculations for the related $\{Ni^{II}-W^V\}$ unit have been performed using the same fragment, simply replacing Mo with W. In both cases, a ferromagnetic interaction was obtained with exchange parameters of $J = +15.5$ cm^{-1} for the $\{Ni-Mo^V\}$ unit and $J = +31.8$ cm^{-1} for the $\{Ni-W^V\}$ unit. These values are in rather good agreement with that found experimentally and well reproduce the increase of the exchange interaction when going from Mo to W.

The three natural magnetic orbitals of the high spin (i.e., quadruplet) state for the $[\{NiL^2\}\{Mo(CN)_8\}]^-$ fragment are shown in Figure 8. Under the name of "magnetic natural orbitals", we refer to natural orbitals with occupancy very close to 1. The molecular orbital of the $\{MoCN_8\}^{3-}$ moiety for the high spin state is the same as that already discussed above (Figure 6) and involves the metal-centered d_{xy} orbital and the π orbitals of the CN ligands. On the Ni side, the MO results from the mixing of the σ system of the ligands (i.e., the macrocycle,

---

(40) Verdaguer, M.; Bleuzen, A.; Train, C.; Garde, R.; Fabrizi de Biani, F.; Desplanches, C. *Philos. Trans. R. Soc. London A* **1999**, *357*, 2959−2976.

(41) Glendening, E. D.; Reed, A. E.; Carpenter, J. E.; Weinhold, F. *NBO 3.1*; University of Wisconsin: Madison, WI, 1996.

(42) Figgis, B. N.; Forsyth, J. B.; Reynolds, P. A. *Inorg. Chem.* **1987**, *26*, 101−105.

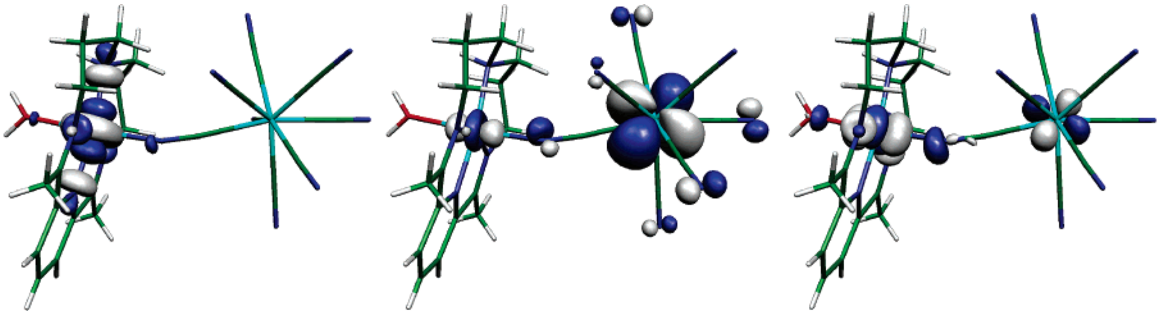

Figure 8. Natural molecular magnetic orbitals of the molecular fragment [Ni(L^2)(H$_2$O)][Mo(CN)$_8$]$^-$.

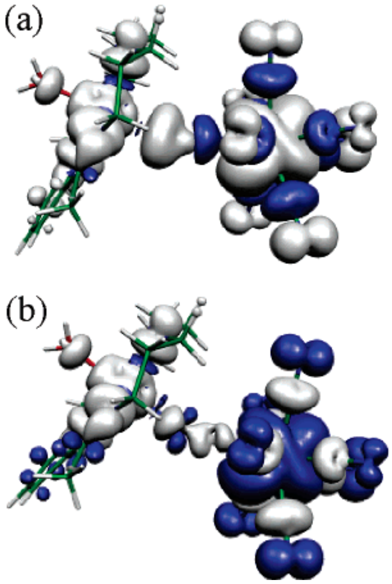

Figure 9. Spin density for the high spin state (a) and the low spin state (b) of the molecular fragment [Ni(L^1)(H$_2$O)][Mo(CN)$_8$]$^-$.

the N-bound CN, and the H$_2$O) with the e$_g$ (d$_{x^2-y^2}$, d$_{z^2}$) of the Ni ion (Figure 8). As expected for a t$_{2g}$^{6} e$_g$^{2} ion, the axes of the orbitals are aligned with the bonds of the Ni with its first coordination sphere. Moreover, the interactions between Ni and the ligands are antibonding, in agreement with classical molecular orbital theory. It can be seen that, for two of the three orbitals (middle and right plots), there is a contribution arising from the two metal centers. Considering that each is delocalized through either a σ or a π system, such mixing should not occur due to the orthogonality of the orbitals. However, because the M−CN→Ni angle deviates from 180° for the molecule considered, a certain amount of mixing may exist.

The spin density distributions computed for the high spin and the low spin states are shown in Figure 9. For the ferromagnetic state (Figure 9a), the spin densities found on the two metal ions have the same sign, whereas they are of different signs for the antiferromagnetic state (Figure 9b). The spin density around the Mo atom is identical to that found for the free [Mo(CN)$_8$]$^{3-}$ unit (Figure 7c). The spin density around the Ni atom has an octahedral shape, with the axis of the octahedron along the Ni−N(O) bonds.

The molecular orbital analysis described above has revealed a strong similarity between the {M(CN)$_8$}$^{3-}$ units and {Cr(CN)$_6$}$^{3-}$. Moreover, their exchange coupling with Ni^{2+} is ferromagnetic. The rationale for the ferromagnetic {Ni−Cr} interaction has been discussed in detail by Verdaguer and coworkers and relies on quasi-orthogonal orbitals.[40,43,44] It takes advantage of Kahn's model,[45] where the exchange parameter J is expressed as the sum of two terms of opposite sign: $J = J_F + J_{AF}$, with $J_F = 2k > 0$ and $J_{AF} = 4\beta s < 0$. In this model, k stands for the bi-electronic exchange integral, β for the mono-electronic resonance integral, and s for the mono-electronic overlap integral. This expression is valid when two centers, each bearing one unpaired electron, are coupled. When several unpaired electrons are present, n_A on one side and n_B on the other side, J can be described by the sum of different orbital pathways, $J_{\mu\nu}$, weighted by the number of electrons: $J = (1/n_An_B)\sum_{\mu\nu} J_{\mu\nu}$. For Cr^{III} and Ni^{II}, the unpaired electrons are delocalized respectively in π- and σ-type orbitals on the bridging cyanide. These localized molecular orbitals have a very small overlap (i.e., $s \approx 0$); therefore, the interaction between Cr^{III} and Ni^{II} is indeed expected to be ferromagnetic. For the {Ni−Mo^V} and {Ni−W^V} interactions considered here, the magnetic information arising from the Mo or W and Ni ions proceeds through the same pathway as for the {Ni−Cr} interaction. Therefore, the same analysis can be applied, leading to the same conclusion. Whether the cyanometalate has square antiprismatic or dodecahedral geometry, the {Ni−Mo^V} and {Ni−W^V} interactions are anticipated to be ferromagnetic. For **1**, the molecular magnetic orbitals (Figure 8) have revealed a slight mixing of contributions arising from each metal center. This indicates that orthogonality is not strict; i.e., the 4βs term is not null, and some antiferromagnetic contribution should exist. At this stage, the open question is about what deviation from the ideal geometry is the rule relating the overall ferromagnetic behavior with the orthogonality of the magnetic orbitals broken? In other words, about what deformation does J_{AF} become larger than J_F? This question has already been discussed in the case of the {Cr−CN−Ni} interaction, and it has been shown that a key parameter governing the strength of the ferromagnetic interaction is the C−N−Ni angle.[46] The value taken by J was found to vary linearly with this angle, and as anticipated, the strongest ferromagnetic interactions are obtained for a 180° angle. An overall antiferromagnetic behavior is predicted only for angles lower than 145°. The C−N−Ni angles occurring in **1a** and **1b** are much above this value; therefore, it seems reasonable to attribute the ferromagnetic interaction observed

---

(43) Gadet, V.; Mallah, T.; Castro, I.; Verdaguer, M. *J. Am. Chem. Soc.* **1992**, *114*, 9213−9214.

(44) Verdaguer, M.; Girolami, G. S. In *Magnetism: Molecules to materials*; Miller, J. S., Drillon, M., Eds.; Wiley-VCH: Weinheim, 2005; Vol. 5, pp 283−346.

(45) Kahn, O. *Molecular Magnetism*; VCH: Weinheim, 1993.

(46) Marvaud, V.; Herrera, J.-M.; Barilero, T.; Tuyeras, F.; Grade, R.; Scuiller, A.; Decroix, C.; Cantuel, M.; Desplanches, C. *Monatsh. Chem.* **2003**, *234*, 149−163.

for these compounds to the quasi-orthogonality of the magnetic orbitals of Ni and Mo(W).

The two main questions addressed in this study are (i) what increase of exchange interaction can be expected when replacing a paramagnetic metal ion with a heavier congener located farther down the periodic table, and (ii) for a molecular unit with higher coordination numbers, i.e., eight in the present case, how is the magnetic information transferred from the metal ion to its ligand set? The first question is, of course, related to the need to improve the properties of molecular assemblies in terms of the persistence of their magnetic features at temperatures suitable for the use of these smart materials in devices. Such improvement mainly requires stronger exchange coupling among the spin carriers. It has been suggested that this might be achieved by using metal ions with more radially extended valence (magnetic) orbitals, but the actual amplitude of the increase remained vague. In the present case, comparison of the strengths of the exchange parameters found for the {Ni−Mo} interaction ($J_{MoNi} = 26.9$ cm^{-1}) in **1a** and the {Ni−W} interaction ($J_{WNi} = 37.3$ cm^{-1}) for the isostructural derivative **1b** clearly shows that the difference is significant. This becomes even more obvious when the related 3d ion, Cr^{III}, is considered, which also has a ferromagnetic interaction with Ni^{II}. A closely related [NiL{Cr(CN)$_6$}] compound[26] has been described to exhibit a {Ni−Cr} coupling of $J = 18.5$ cm^{-1}. This compound exhibits Ni−NC−M distances and angles very similar to those of **1** (see Supporting Information), which allows us to exclude geometrical considerations as the origin of the difference in the interaction strengths. Thus, the anticipated increase of the exchange interaction for 4d and subsequently 5d metal ions is demonstrated experimentally. For the series Cr^{III}, Mo^{V}, W^{V}, the strength of the coupling with Ni^{II} is increased by ca. 10 cm^{-1} on moving from Cr to Mo and a further 10 cm^{-1} between the Mo and W derivatives, the exchange parameter with the 5d ion, J_{NiW}, being twice that of the interaction with the 3d ion, J_{NiCr}. The origin of the difference in exchange coupling capability is found in the transfer of the magnetic information from the metal center to its ligand set. The spin density distribution for the {M(CN)$_8$}$^{3-}$ unit (Table 4) clearly shows that the magnetic information is more delocalized from the metal ion onto the cyanides for the W than for the Mo. With the 5d ion, the spin densities located on the N atoms are about 20% larger than those found for the 4d derivative, exceeding also those obtained for the [Cr(CN)$_6$]$^{3-}$ unit that possesses a spin of $S = {}^3/_2$. This propensity for spin delocalization can be attributed to a better overlap of the ligand and metal orbitals as a result of the enlarged spatial extension of the valence (magnetic) orbitals for the metal ion following the trend 3d < 4d < 5d. For the {Mo−Ni} and {W−Ni} derivatives **1a** and **1b** investigated here, 20% more spin density on the bridging ligand resulted in an exchange interaction that was increased by 10 cm^{-1}, a value that represents ca. 37% of the initial exchange parameter. The computed interaction parameters for a [{NiL^2}{M(CN)$_8$}]$^-$ fragment ($J = 15.5$ cm^{-1} and $J = 31.8$ cm^{-1}, respectively, for Mo and W) confirm the correlation between the spin located on the bridging ligand and the strength of the exchange coupling.

Turning to the second initial question, about the transfer of the magnetic information for eight-coordinated {M(CN)$_8$} species, there is a fundamental importance in understanding the interaction pathways when analyzing the magnetic behavior of an architecture involving this unit. The incidence of the actual geometry of a paramagnetic {M(CN)$_8$} unit (M = Mo^V, W^V, Nb^{IV}, ...) is usually ignored when the magnetic behavior of exchanged coupled systems is analyzed. It is generally considered that all eight cyanide ligands are perfectly equivalent. But this is the case only when {M(CN)$_8$} has a square antiprismatic geometry; a dodecahedral geometry has two types of cyanide sites, and a bicapped trigonal prism has three different sites. For a d^1 electronic configuration with a single magnetic orbital, the overlap between the ligand orbitals and the metal orbital bearing the unpaired electron will be different for ligands of different sites. The direct consequence of this can be found in Table 4, where the spin density distributions on {Mo(CN)$_8$} are reported for these geometries. For the DD geometry, the spin densities found on the CN sitting on the A site is only 40% that of the cyanide located on B sites (+0.00267 versus +0.0649). As a result, the exchange interaction mediated by a CN on a B site will be stronger than the interaction mediated by a CN sitting on an A site. This is indeed observed experimentally and accounts for the differences found between **1a**,**b** ($J_{MoNi} = 26.9$ cm^{-1} and $J_{WNi} = 37.3$ cm^{-1}) and **2a**,**b** ($J_{MoNi} = 15.4$ cm^{-1} and $J_{WNi} = 14.2$ cm^{-1}). For both **1** and **2**, the {M(CN)$_8$} units have a shape close to DD geometry, but whereas the cyanide ligands bridging the Mo/W and the Ni ions are sitting on B-type sites for **1**, they are located on A-type sites for **2**. In a recent DFT investigation on a [{Mo^V(CN)$_8$}-Mn^{II}] system, Ruiz et al.[47] found exchange parameters of $J = -12$ cm^{-1} through A-type cyanides and $J = -20$ cm^{-1} through B-type cyanides. Thus, in DD geometry or closely related shapes, the cyanides on A and B sites must be considered as two different exchange pathways. It can be noticed that, for the SAP geometry, the spin density borne by the CN ligand is between those found for the A and B sites in the DD; therefore, exchange coupling in the case of a d^1 SAP {M(CN)$_8$} unit is anticipated to be intermediate as well.

Examination of the molecular orbitals for the {M(CN)$_8$} unit (Figure 6) and the distribution of the spin density (Figure 7) revealed that the transfer of the magnetic information from the central metal proceeds mainly through π-orbitals of the cyanide ligands. This pathway is independent of whether the unit has DD or SAP geometry and applies for all CN ligands. Knowledge of the orbitals involved in the exchange interaction makes it possible to rationalize and design a magnetic behavior. We have discussed above the rationale for the observed ferromagnetic {Mo−Ni} and {W−Ni} interactions, pointing out that a parallel can be drawn between the d^1 {M(CN)$_8$} units and {Cr(CN)$_6$}$^{3-}$. This applies for the interaction with Ni^{II} but should remain true also for other metal ions. The ferro- or antiferromagnetic nature of the exchange interaction involving {M(CN)$_8$} units (M = ion in d^1 configuration) in DD, SAP, or related shapes should follow the rules[48] that apply for {Cr(CN)$_6$}$^{3-}$.

Concluding Remarks

The qualitative and quantitative information gathered clearly confirms that the strength of the exchange interaction increases

---

(47) Ruiz, E.; Gopalan, G.; Alvarez, S.; Gillon, B.; Stride, J.; Clérac, R.; Larionova, J.; Decurtins, S. *Angew. Chem., Int. Ed.* **2005**, *44*, 2711−2715.

(48) Verdaguer, M.; Bleuzen, A.; Marvaud, V.; Vaissermann, J.; Seuleiman, M.; Desplanches, C.; Scuiller, A.; Train, C.; Garde, R.; Gelly, G.; Lomenech, C.; Rosenman, I.; Veillet, P.; Cartier, C.; Villain, F. *Coord. Chem. Rev.* **1999**, *190−192*, 1023−1047.

significantly with the radial extension of the valence (magnetic) orbitals of the metal ions, following the sequence 3d < 4d < 5d. This enhanced coupling is directly related to a larger density of spin spread out from the metal onto the ligand set as we go down the column in the periodic table. In the present study, we have considered the ferromagnetic exchange coupling with Ni^{II}, which results from non-overlapping magnetic orbitals. A larger amplitude of exchange strengthening can be expected for a metal ion having its magnetic orbitals overlapping with those of the $\{M(CN)_8\}$ unit.

This study also underlines that, for molecular units with higher coordination numbers, eight in the present case, an accurate analysis of the magnetic behavior necessitates taking into consideration the geometry of the unit. Indeed, for the $\{M(CN)_8\}$ unit, the amount of spin density borne by the ligands has been found to vary as $DD_{B\ site} > SAP > DD_{A\ site}$. The exchange interactions with this unit should follow the same trend. Finally, when the polyhedron possesses nonequivalent CN sites, as is the case for a dodecahedron, the strength of the exchange interaction is significantly affected by the location of the bridging ligands.

Experimental Section

General. The $Cs_3[Mo(CN)_8]\cdot 2H_2O$,[49] $(TBA)_3[W(CN)_8]\cdot 2H_2O$,[49] and $\{NiL^2\}(ClO_4)_2$[50] were prepared according to the literature methods. The IR spectra (KBr pellets) were recorded with a Perkin-Elmer FT-IR Paragon 1000 spectrophotometer in the range 4000−400 cm^{-1}. All solvents were distilled prior to use. Chemical analyses were performed by the "Service Central d'Analyse du CNRS" at Vernaison, France. Magnetic susceptibility measurements were carried out with a Quantum Design MPMS-5S SQUID magnetometer. All magnetic data were corrected for core diamagnetic contributions estimated from Pascal tables and for the sample holder (gelatin capsule) contribution.

Syntheses. $[\{NiL^2(H_2O)\}_2\{Mo(CN)_8\}](ClO_4)$ (1a). A solution of $Cs_3[Mo(CN)_8]\cdot 2H_2O$ (27 mg, 0.041 mmol) in H_2O acidified to pH = 2−3 with $HClO_4$ was layered with an aqueous solution of the $\{NiL^2\}(ClO_4)_2$ (44 mg, 0.085 mmol). Slow interdiffusion yielded 1a (10 mg; yield 21%) as amber, platelike single crystals. Analysis calculated (found) for $C_{38}H_{52}N_{16}O_8Ni_2MoCl$: C, 41.13 (40.93); H, 4.72 (4.98); N, 20.20 (20.23). IR (KBr, cm^{-1}): 3443 (s), 3264 (s), 2930 (m), 2881 (w), 2153 (m), 2144 (m), 2126 (w), 1620 (m), 1583 (m), 1428 (m), 1261 (m), 1206 (m), 1108 (s), 1080 (s), 1082 (s), 1042 (w), 908 (w), 815 (m), 627 (m).

$[\{NiL^2(H_2O)\}_2\{W(CN)_8\}](ClO_4)$ (1b). The same procedure as for **1a** was used but starting from $(TBA)_3[W(CN)_8]\cdot 2H_2O$ (31 mg, 0.041 mmol) in MeOH acidified to pH = 2−3 with $HClO_4$. Slow interdiffusion yielded **1b** (22 mg; yield 44%) as amber, platelike crystals. Analysis calculated (found) for $C_{38}H_{56}N_{16}O_{10}Ni_2WCl$: C, 37.00 (37.35); H, 4.58 (4.63); N, 18.16 (17.98). IR (KBr, cm^{-1}): 3449 (m), 3269 (w), 2927 (w), 2846 (w), 2155 (m), 2146 (m), 2130 (w), 1618 (m), 1538 (m), 1426 (m), 1261 (m), 1206 (s), 1146 (s), 1121 (s), 907 (m), 815 (m), 626 (m).

$[\{NiL^2\}\{Mo(CN)_8\}_2]\{NiL^2(H_2O)_2\}_2$ (2a). Slow interdiffusion of a solution of $Cs_3[Mo(CN)_8]\cdot 2H_2O$ (19 mg, 0.025 mmol) in 10 mL of H_2O and a solution of $\{NiL^2\}(ClO_4)_2$ (27 mg, 0.050 mmol) in 15 mL of H_2O yielded **2a** as plate-shaped, red-brown single crystals. Analysis calculated (found) for $C_{61}H_{80}N_{28}O_7Ni_3Mo_2$: C, 43.47 (43.17); H, 4.78 (4.84); N, 23.27 (23.10). IR (KBr, cm^{-1}): 3362 (s), 3270 (m), 3090 (m), 2930 (m), 2870 (m), 2177 (w), 2159 (m), 2145 (m), 2110 (w), 1621 (s), 1585 (m), 1466 (m), 1425 (m), 1355 (m), 1260 (m), 1205 (m), 1072 (m), 1045 (m), 909 (w), 812 (m). Crystal data obtained at 293 K: orthorhombic, $a = 14.278$ (1) Å, $b = 14.309(1)$ Å, $c = 37.896(1)$ Å, $V = 7743(1)$ Å^3.

$[\{NiL^2\}\{W(CN)_8\}_2]\{NiL^2(H_2O)_2\}_2$ (2b). The same procedure as for **2a** was used except that $(TBA)_3[W(CN)_8]\cdot 2H_2O$ (15 mg, 0.02 mmol) was dissolved in slightly acidified (pH > 3) MeOH. Plate-shaped, red-brown single crystals of **2b** were obtained within one week (yield 30%). Analysis calculated (found) for $C_{61}H_{76}N_{28}Ni_3Mo_2 + 3MeOH + 5 H_2O$: C, 39.80 (39.74); H, 5.11 (4.58); N, 20.30 (20.12). IR (KBr, cm^{-1}): 3430 (s), 3200 (s), 3085 (m), 2936 (m), 2868 (m), 2181 (w), 2164 (m), 2146 (m), 1621 (m), 1585 (m), 1473 (m), 1426 (m), 1356 (m), 1272 (m), 1261 (m), 1206 (m), 1074 (w), 1045 (w), 906 (w), 813 (w), 794 (w). Crystal data obtained at 293 K: orthorhombic, $a = 14.295(1)$ Å, $b = 14.348(1)$ Å, $c = 37.920(2)$ Å, $V = 7778(1)$ Å^3.

Crystallographic Studies. The single-crystal diffraction data were collected on a Nonius Kappa CCD diffractometer at 298 K using Mo Kα graphite-monochromated radiation (λ(Mo Kα) = 0.71069 Å). For all compounds, the structure was solved by direct methods using the program SHELXS-97. The refinement and all further calculations were carried out using SHELXL-97. The H atoms were included in calculated positions and treated as riding atoms using SHELXL default parameters. The non-H atoms were refined anisotropically, using weighted full-matrix least-squares on F^2. Crystallographic data are summarized in Table 1.

DFT Calculations. Calculations were carried out on $[Mo(CN)_8]^{3-}$ moieties for ideal SAP (D_{4d}) and DD (D_{2d}) geometries, as well as for experimental geometry at crystallographic coordinates. For ideal geometries, we assume a constant Mo−C distance of 2.15 Å, a constant C−N distance of 1.14 Å, and perfectly linear Mo−C−N angles. The improper rotation axis (S_8 for SAP, S_4 for DD) was set along the z axis. For DD geometry, all the ligand atoms were assumed to be either in the $x = 0$ plane or in the $y = 0$ plane. Once the distances Mo−C and C−N is fixed, the shape of a dodecahedron is specified by two angles, θ_A and θ_B, between nonequivalent atoms and the z axis. In this so-called hard-sphere idealization,[51] θ_A and θ_B have values of 36.85° and 69.46°, respectively. For the SAP geometry, only one angle with $\theta = 59.26°$ is required. These values have been used to fix the reference geometries of the $\{M(CN)_8\}$ unit considered in our study. In addition, $[Cr(CN)_6]^{3-}$ was scrutinized using DFT techniques. This unit was chosen to be perfectly octahedral, with Cr−C and C−N distances of 2.06 and 1.14 Å, respectively.

Computational Methodology. Standard DFT calculations have previously been used for the evaluation of exchange coupling constants for transition metal dimers, including some of the second-row transition series.[47,52−54] For each coupling constant, two separate DFT calculations were carried out, one for the highest spin state (quadruplet state for the species considered here) and one for the broken-symmetry state. The hybrid B3LYP[55] functional was used as implemented in Gaussian98.[56] The basis used in all calculations is the D95 Dunning−Huzinaga valence double-ζ[57] for first-row elements and the small-core Hay−Wadt pseudopotential[58] for transition metals (indicated in the Gaussian code as LANL2DZ). The J values were then obtained by considering $E_{HS} - E_{BS} = -J(2S_1S_2 + S_2)$, where S_1 and S_2 are the spins the two metal centers ($S_1 > S_2$ has been assumed) and E_{HS} and E_{BS} are the energies of high spin and broken-symmetry states, respectively. We assumed that the energy of the broken-symmetry state is a good

---

(49) Dennis, C. R.; van Wyk, A. J.; Basson, S. S.; Leipoldt, J. G. *Transition Met. Chem.* **1992**, *17*, 471−473.

(50) Karn, J. L.; Busch, D. H. *Inorg. Chem.* **1969**, *8*, 1149−1153.

(51) Hoard, J. L.; Silverton, J. V. *Inorg. Chem.* **1963**, *2*, 235−242.

(52) Desplanches, C.; Ruiz, E.; Alvarez, S. *Eur. J. Inorg. Chem.* **2003**, 1756−1760.

(53) Low, D.; Rajaraman, G.; Helliwell, M.; Walsmann, O.; Gudel, H.; Adams, M.; Ruiz, E.; Alvarez, S.; McInnes, E. *Chem. Eur. J.* **2006**, *12*, 1385−1396.

(54) Ruiz, E.; Nunzi, F.; Alvarez, S. *Nano Lett.* **2006**, *6*, 380−384.

(55) Becke, A. D. J. *J. Chem. Phys.* **1993**, *98*, 5648−5652.

(56) Frisch, M. J.; et al. *Gaussian98*; Gaussian, Inc.: Pittsburgh, PA, 1998.

(57) Dunning, T. H. J.; Hay, P. J. In *Modern Theoretical Chemistry*; Schaefer, H. F., III, Ed.; Plenum: New York, 1976; Vol. 3.

(58) Hay, P. J.; Wadt, R. *J. Chem. Phys.* **1985**, *82*, 299−310.

approximation of low spin state energy, following Ruiz et al.[59,60] Spin population analyses were carried out with the Gaussian code in the NBO framework.[41] The natural orbitals represented here were computed with Gaussian98.[61]

Acknowledgment. The authors are grateful to Prof. S. Alvarez from the University of Barcelona, Spain, for performing the continuous shape measures analysis for **1** and **2**. This work was supported by the European Union sixth framework program NMP3-CT-2005-515767, entitled “MAGMANet: Molecular Approach to Nanomagnets and Multifunctional Materials”, and by the Centre Franco-Indien pour la promotion de la Recherche Avancée/Indo-French Centre for the Promotion of Advanced Research (Project 3108-3). The computing resources were generously made available by the CINES. The authors are grateful to the French Ministries of Research and of Foreign Affairs for the research grants to I.I., R.P., and F.A.V.

Supporting Information Available: Complete ref 56; crystallographic information in CIF format for **1a**,**b**; ORTEP plots with numbering scheme, bond lengths, and angles for **1a**,**b**; view of the molecular structure of **2a**,**b**; view of the supramolecular H-bonded organization for **1a**,**b** and **2a**,**b**; magnetic behavior for **2b**. This material is available free of charge via the Internet at http://pubs.acs.org.

JA061911X

---

(59) Ruiz, E.; Cano, J.; Alvarez, S.; Alemany, P. *J. Comput. Chem.* **1999**, *20*, 1391−1340.

(60) Ruiz, E.; Alvarez, S.; Cano, J.; Polo, V. *J. Chem. Phys.* **2005**, *1234*, 164110.

(61) Löwdin, P.-O. *Phys. Rev.* **1955**, *97*, 1474−1489.